Water flow processes in a soil column with a cylindrical macropore: Experiment and hierarchical modeling

J. Maximilian Köhne and Binayak P. Mohanty

Department of Biological and Agricultural Engineering, Texas A&M University, College Station, Texas, USA

Received 27 April 2004; revised 21 November 2004; accepted 13 January 2005; published 16 March 2005.

[1] Physically based models are increasingly applied to analyze contaminant transport in soil by preferential water flow. Unfortunately, in the past, preferential flow models were rarely evaluated using appropriate experimental data because of the complexity of conceptual models and limitations of measuring techniques. In this study, we designed a novel soil column experiment with advanced measurement techniques that enabled us to discriminate macropore and matrix water flow and quantify interdomain (macropore-matrix) water transfer. Experiments of drainage and upward and downward infiltration revealed hydraulic nonequilibrium between matrix and macropore domains. Cumulative interdomain water transfer could be estimated using mass balance calculations. In a hierarchical modeling approach, four numerical models of different complexity were compared to the column experiment data. As a reference model, pseudo three-dimensional axisymmetric Richards' equation (ARE) was used for inverse estimation of domain-specific hydraulic parameters. The parameters were subsequently used for performance evaluation of an equivalent continuum model with bimodal hydraulic functions (ECM) and two dual-permeability models with first-order (DPM1) and second-order (DPM2) terms for water transfer between macropore and matrix. Overall, DPM2 gave slightly more accurate domain-specific results of water flow, water contents, and pressure heads than DPM1. Although bulk soil water flow results for the ECM were least accurate, they were considered to be within acceptable range. Compared to the more comprehensive ARE approach, DPMs were found to be almost equally capable of simulating interdomain and intradomain water flow and could be considered more versatile as they allow for a variety of macropore-matrix geometries.

Citation: Köhne, J. M., and B. P. Mohanty (2005), Water flow processes in a soil column with a cylindrical macropore: Experiment and hierarchical modeling, *Water Resour. Res.*, *41*, W03010, doi:10.1029/2004WR003303.

1. Introduction

[2] Undisturbed structured soil columns have frequently been used in the lab to study preferential flow and transport under controlled conditions. Unfortunately, the complexity of the soil structure prohibits explicit insight into the processes involved. In order to better understand preferential flow processes, constructed soil-macropore systems of known geometry have been studied [e.g., *Bouma and Anderson*, 1977; *Ela et al.*, 1992; *Li and Ghodrati*, 1997]. However, in the past even the experimental findings using well-defined artificial macropore-soil systems were difficult to interpret. For instance, *Ela et al.* [1992] found no relation between infiltration rate and macropore diameter (between 0.2 and 0.5 cm). In another study [*Ahuja et al.*, 1995], bottom outflow measurements of a soil column containing a 0.3 cm artificial macropore could only be simulated with the root zone water quality model (RZWQM) when assuming restricted water transfer between macropore and matrix. *Li and Ghodrati* [1997] measured nitrate transport through soil containing several artificial 0.3 cm macropores. Breakthrough curves exhibited double peaks for high water flux, while for smaller flux the breakthrough curves displayed single peaks. Double peaks were tentatively attributed to transport through macropores and matrix, respectively [*Li and Ghodrati*, 1997]. Even if all above mentioned studies were based on artificial soil-macropore systems, explanations for the processes underlying some of the observed phenomena remained hypothetical and qualitative in nature.

[3] Recently there have been increased efforts to obtain more direct information on flow and transport in macropores and matrix domains. *Logsdon* [1995] designed a column for sampling gravity outflow separately from matrix and a macropore. *Ghodrati et al.* [1999] used a semicylindrical macropore column to visually study macropore flow mechanisms at the planar split column surface using dye tracers and effluent breakthrough curves. Similarly, a rectangular plate chamber with five outlets for leachate sampling was constructed to study effluent breakthrough curves from tracer tests with macroporous soil and to visually observe dye tracer transport as influenced by macropore continuity [*Allaire-Leung et al.*, 2000a] and macropore tortuosity [*Allaire-Leung et al.*, 2000b]. In a recent study, the depth-integrated water exchange between matrix and a centrally located macropore was analyzed with an infiltration experiment making use of a flow interruption method [*Castiglione et al.*, 2003].

0043-1397/05/2004WR003303$09.00

[4] Various models have been developed to assess the risk of groundwater contamination by preferential flow mechanisms in soil. *Mohanty et al.* [1997] applied an equivalent continuum model with composite piecewise continuous hydraulic functions fitted to data from a macroporous field soil and applied it successfully for predicting preferential flow to a tile drain in the field. Other models rely on a dual-permeability concept and assume validity of Richards' equation to describe water flow in both pore domains [e.g., *Gerke and van Genuchten*, 1993a; *Ray et al.*, 1997]. However, only very few studies have reported direct evaluation of preferential flow models using experimental data [*Allaire et al.*, 2002a, 2002b; *Castiglione et al.*, 2003]. For thorough evaluation of the existing preferential flow models, experimental data for domain-specific water flow in a macroporous soil with well-defined geometry, initial and boundary conditions are required.

[5] This study has two main objectives: (1) to quantify the preferential flow components in matrix domain, macropore domain, and the between-domain exchange utilizing a novel experimental setup with a cylindrical macropore at the centre of a repacked soil column, and (2) test one single-domain and two dual-domain preferential flow models using parameters obtained by inverse solution of pseudo three-dimensional axisymmetric Richards' equation and identify the degree of model complexity needed to describe the experimental data of preferential flow in the macroporous soil.

2. Experimental Approach

2.1. Column Setup

2.1.1. Artificial Macropore Design

[6] The novel experimental setup (Figure 1) included a large (24.4 cm diameter, 80 cm long) acrylic column with a perforated PVC plate (2 holes of 0.3 cm diameter per cm^2) at the bottom, covered with a nylon membrane (30 μm mesh size), a central cylindrical flow divider (2.4 cm diameter, 5 cm height) to minimize lower boundary effects on water exchange flux between macropore and matrix, and separate outlets for macropore and matrix effluent. During the soil column preparation, a metal tube of 2.4 cm diameter was vertically attached to the flow divider (Figure 1) and coarse sand (Table 1) was poured into it, resulting in a 2.4 cm diameter macropore filled with sand at a relatively low bulk density of 1.41 g/cm^3. The reason for filling the macropore with sand was to attain continuous water retention and hydraulic conductivity functions of the macropore as required by our model analyses based on continuum theory (see below). The relatively large diameter of the macropore was chosen to facilitate measurements of pressure head and water content inside the macropore domain without stemming the flow inside the macropore. Conceptually, the loosely filled macropore represents a preferential flow path (porous medium) like, for instance, a large vertical earthworm burrow or decayed root channel partially refilled with loose soil.

[7] The column was packed with dry-sieved and graded sandy loam soil (Table 1) sampled from an agricultural field soil near College Station, Texas. It was packed in 3 cm increments to a constant bulk density of 1.59 g/cm^3 equal to that of the natural field soil. After both matrix and macropore domains were established, the metal tube separating macropore and soil matrix was slowly pulled out of the column.

2.1.2. Profile Water Content and Pressure Monitoring

[8] In the column, 5 time domain reflectometry (TDR) three-prong probes (8 cm long, 1.1 cm spacing between rods) were inserted into the sandy loam matrix at 5 cm, 20 cm, 35 cm, 50 cm and 65 cm depths from the top (Figure 1). Additionally, 4 small TDR coil probes were built according to the design of *Nissen et al.* [1998]. The TDR coil probes were only 3 mm in diameter and the lacquer-coated copper coil was 21 mm long. TDR coil probes have been used recently to monitor the spatiotemporal evolution of unstable wetting fronts because of finger flow, another manifestation of preferential flow, in sandy soils [*Nissen et al.*, 1999]. Since fingers forming during unstable flow in coarse sand have diameters of at least 4.5 cm [*Wang et al.*, 2003], the flow in the coarse sand within our 2.4 cm diameter macropore can be assumed as stable. In this study, because of their small size, TDR coil probes were used for measuring flow within the macropore domain. Two sets of TDR coil probes were placed at two depths of 20 cm and 35 cm with the coil placed (1) inside the macropore and (2) in the matrix at 2 cm from the macropore wall (Figure 1). The TDR probes were calibrated for measuring water contents in the loamy matrix and TDR coil probes were calibrated for both loamy matrix and sand-filled macropore. Corresponding to the 5 TDR probe positions (at 5 cm, 20 cm, 35 cm, 50 cm and 65 cm depth), tensiometers with 2 mm diameter ceramic cup (SDEC 220, SDEC France) were inserted into the sand-filled macropore. Another set of tensiometers with 6 mm diameter ceramic cup (SDEC 230, SDEC France) were installed in the soil matrix at 6 cm and 2 cm distance from the macropore wall, respectively (Figure 1). To check for any suction loss across the lower boundary of the soil column, another tensiometer recorded the pressure head in the soil matrix at the depth of 79 cm. All tensiometers were equipped with pressure transducers (Microswitch, Soil Measurement System, Tucson, AZ) for automated domain-specific pressure monitoring.

2.1.3. Top and Bottom Boundaries and Flux Monitoring

[9] The top boundary condition (pressure head) for the soil column was maintained using a disc infiltrometer (Zwickert Feinmechanik, Kiel, Germany) of matching diameter (24 cm). The tension infiltrometer was automatically refilled if the water column in the measurement tower decreased below a minimum level as monitored by a differential pressure transducer (PX26-001, Omega Engineering Inc., Stamford, CT). For refilling, a solenoid valve (Granzow Inc., Charlotte, NC) closed the water line between infiltrometer and disc, while another solenoid valve opened the water line between measurement tower and water supply tank, and a third valve opened a connection between measurement tower and vacuum tank to accelerate refilling and to assure equilibrium to the preinstalled suction before reopening the valve to the infiltration disc. At the bottom of the soil column, suctions between 0 cm and 30 kPa could be applied. Suctions were controlled by a vacuum gauge (VR3600, Squire Cogswell, Gurnee, IL) attached to a 38 L tank installed as a vacuum buffer between soil column and vacuum pump. The vacuum tank effectively reduced pressure fluctuations in the vacuum system. Out-

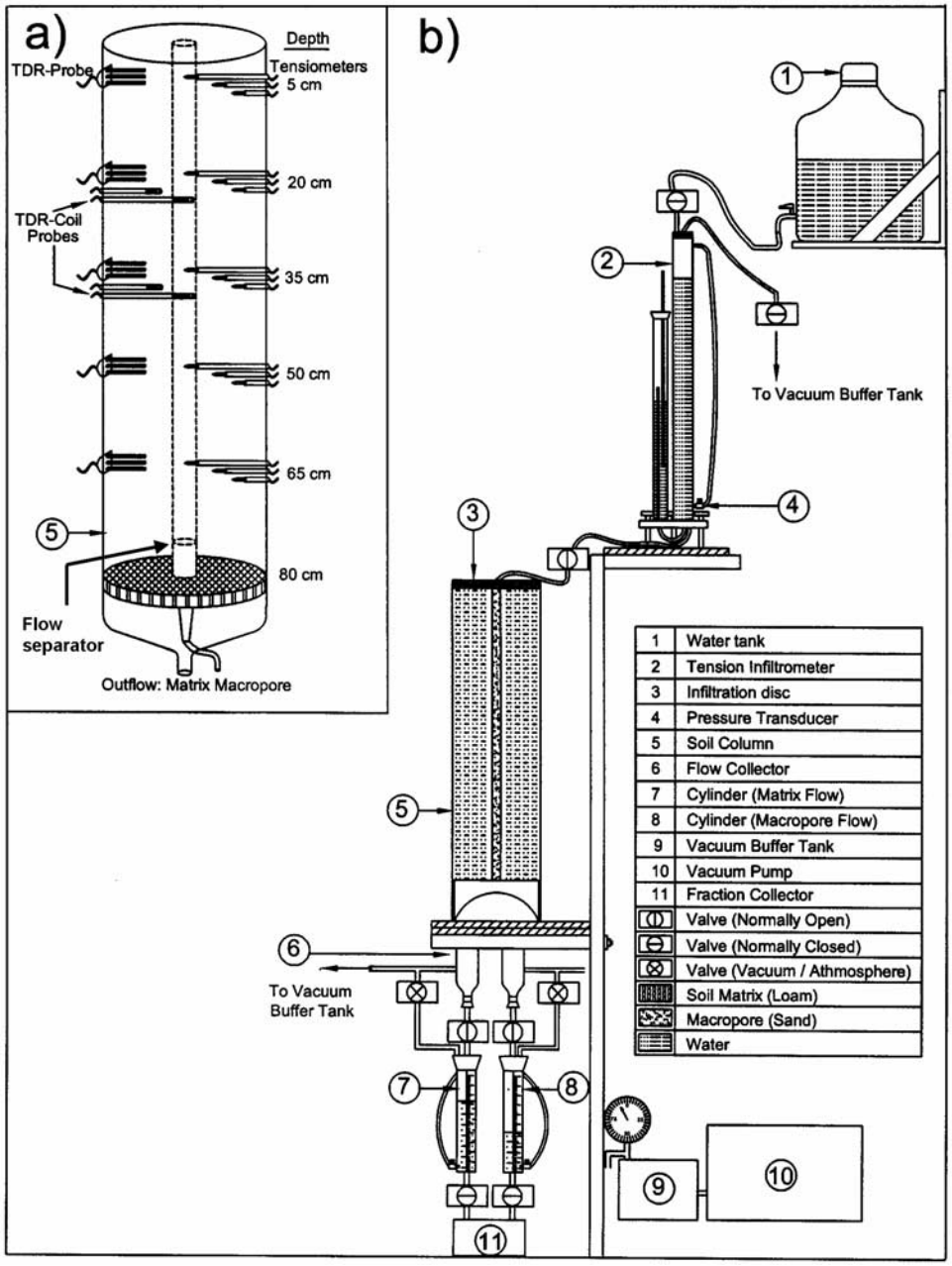

Figure 1. Soil column setup for studying macropore flow processes: (a) column with instrumentation and (b) complete setup.

flow from matrix and macropore was monitored in two separate effluent cylinders. A system of 3 valves per outlet automatically controlled emptying of the effluent cylinders without interrupting the suction connection to the outlets. The arrangement minimizes the disturbances of boundary conditions critical for measuring flow in multidomain pore systems in a continuous manner. Two air vents at 20 cm and 60 cm depth on the column wall minimized effects of air entrapment. Air vents were closed as soon as water started to drip out of them. The experimental setup was controlled and

Table 1. Physical Properties of the Matrix Domain (Sandy Loam) and Macropore Domain (Coarse Sand)

	Texture Properties, Percent by Weight						
Pore Domain	2–0.5 mm Coarse Sand	0.5–0.2 mm Medium Sand	0.2–0.05 mm Fine Sand	0.05–0.002 mm Silt	<0.002 mm Clay	Organic Carbon, %	Bulk Density ρ, g cm^{-3}
Matrix	0.0	0.6	52.5	35.8	11.1	0.24	1.59
Macropore	87.8	11.3	0.9	0	0	n.a.	1.41

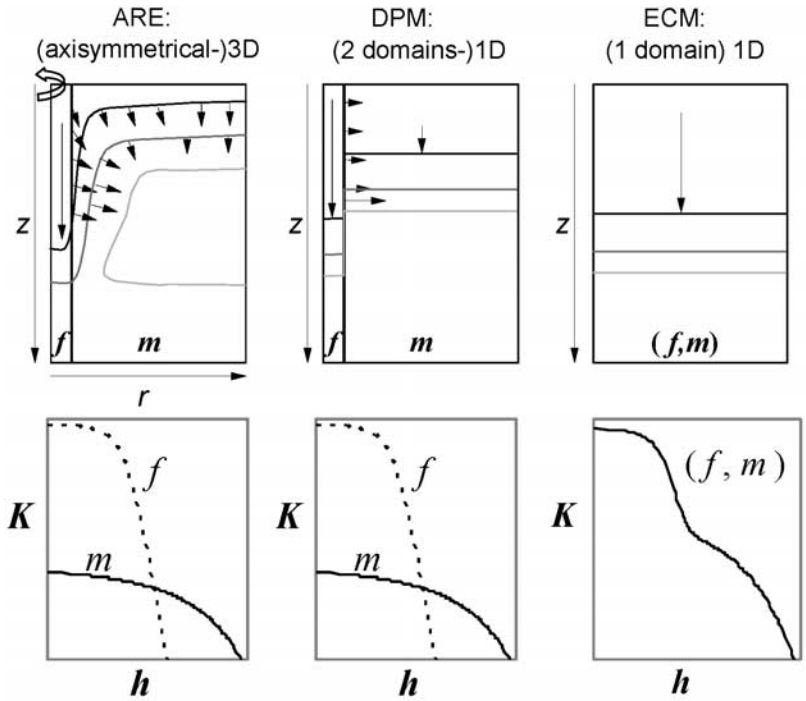

Figure 2. Schematic representation of the conceptual models axisymmetric Richards' equation (ARE), dual-permeability model (DPM), and equivalent continuum model (ECM). Symbols: z, depth coordinate; r, radial coordinate; K, hydraulic conductivity; h, pressure head; m, matrix; f, macropore; (f, m), composite macroporous medium.

monitored using several equipments from Campbell Scientific, Inc. (Logan, UT), consisting of 2 CR10X data loggers with an AM 16/32 multiplexer for pressure transducers, a TDR100 with 2 SDMX50 multiplexers, and two relay drivers A6-REL12. Experiments were conducted in a lab with ambient air temperature of 22° ± 2°C.

2.2. Column Experiments

[10] After duplicate experiments under various initial and boundary conditions were conducted with repeatable results, three flow experiments were analyzed and presented in this study: (1) drainage, (2) infiltration, and (3) upward infiltration. For the drainage experiment, the soil was initially fully saturated. The top of the column was covered with a plastic sheet to minimize evaporation, and the experiment was initiated by opening the outlet valves of both macropore and matrix domains simultaneously.

[11] Prior to the infiltration experiment, the column was drained and left open at the top to the atmosphere for one week, followed by another week in which the top boundary of the column was covered, which resulted in a field-capacity type initial soil moisture condition. The corresponding pressure profile ranged between $h = -140$ cm near the top and $h = -60$ cm near the bottom of the column. Water was infiltrated with a constant pressure head ($h = 0$) top boundary condition, while the bottom outlets were open to atmospheric pressure. The top boundary of the column was covered with a plastic sheet for minimizing evaporative loss.

[12] For the upward infiltration experiment, initial conditions were kept similar as for the (downward) infiltration experiment. A ponded head of +77 cm was maintained at the bottom boundary of the macropore domain using a Mariotte bottle that was placed on a balance recording the cumulative upward infiltration. The matrix domain bottom boundary was kept closed to be able to quantify water transfer between macropore and matrix during the upward infiltration.

3. Conceptual Models

[13] The three conceptual models used in this study are illustrated in Figure 2 assuming a fictitious infiltration scenario. The ARE approach calculates the axisymmetric 3-D flow field within and across two concentric cylinders with distinctly different hydraulic properties representing the macropore and the matrix domains. The DPM approach approximates the flow field assuming two 1-D vertical domains coupled by a dimensionless water transfer term. Macropore and matrix domains are represented by separate hydraulic functions as for the ARE approach. The ECM approach assumes equilibrium flow in one composite domain. Characteristic composite hydraulic functions are assumed that represent the bimodal pore size distribution of a soil consisting of macropores and micropores (matrix) (Figure 2). While ECM is the simplest conceptual approach used in this study for describing preferential flow, it is superior to any single-domain flow model which assumes hydraulic functions based on unimodal pore size distribution. The ECM approach, however, can not account for preferential solute transport where part of the solute bypasses the soil matrix.

3.1. Axisymmetric Richards' Equation

[14] The ARE approach was based on the Richards' equation in cylindrical coordinates describing vertical,

Table 2. Initial and Boundary Conditions (BC) for Simulation of the Three Experiments[a]

Experiment	Initial Condition[b]	Upper BC	Lower BC
Infiltration	$h(r, L, 0) = -60$ cm $h(r, 0, 0) = -140$ cm	$h(r, 0, t) = 0$	$q(r, L, t) = 0$, if $h(r, L, t) < 0$ $h(r, L, t) = 0$, else[c].
Upward infiltration	$h(r, L, 0) = -45$ cm $h(r, 0, 0) = -115$ cm	$q(r, 0, t) = -0.5$ cm/d[d]	$h(r, L, t) = 77$ cm, $0 < r < 1.2$ cm[e] $q(r, L, t) = 0$, $1.2 \leq r < 12.2$ cm[f]
Drainage	$h(r, L, 0) = 80$ cm $h(r, 0, 0) = 0$	$q(r, 0, t) = 0$	$q(r, L, t) = 0$, if $h(r, L, t) < 0$ $h(r, L, t) = 0$, else[c].

[a]Symbols: h, pressure head; q, flux; r, radial coordinate; L, column length (80 cm); t, time.
[b]Equilibrium profile with h values linearly interpolated for depths between 0 and L.
[c]These conditions represent a seepage face boundary condition [*Simunek et al.*, 1999].
[d]Evaporation.
[e]Constant pressure head in the macropore domain.
[f]Zero water flux in the matrix domain.

pseudo 3-D axisymmetric, variably saturated flow in a rigid isotropic porous medium neglecting effects of air phase on water flow

$$\frac{\partial \theta}{\partial t} = \frac{\partial}{\partial r}\left(K\frac{\partial h}{\partial r}\right) + \frac{\partial}{\partial z}\left(K\frac{\partial h}{\partial z} + K\right) \tag{1}$$

where θ is the volumetric water content (L^3L^{-3}), h is the pressure head (L), t is time (T), r is the radial coordinate (L), z is the vertical coordinate (positive upward), and K is the unsaturated hydraulic conductivity function (LT^{-1}) given by

$$K(h, r, z) = K_s(r, z)K_r(h, r, z) \tag{2}$$

where K_r is the relative hydraulic conductivity and K_s the saturated hydraulic conductivity (LT^{-1}). Equation (1) was solved with a mass lumped Galerkin finite element scheme with triangular elements using HYDRUS-2D [*Simunek et al.*, 1999]. A rectangular grid comprising two vertical domains with different hydraulic properties was assumed to represent the central cylindrical macropore of 1.2 cm radius surrounded by the cylindrical matrix mantle of 11 cm radius. The numerical grid was discretized into 4830 nodes with 0.4 cm vertical spacing and variable horizontal spacing with a minimum of 0.03 cm increasing with distance from the matrix-macropore interface. For the model evaluation, initial and boundary conditions (Table 2) were derived from the column experiments.

[15] The functions $\theta(h)$ and $K(\theta)$ for the matrix and the macropore domain were parameterized with the *van Genuchten* [1980] model using inverse estimation. Inverse estimation allows the best possible model description of experimental data and hence is better suited for model evaluation than using independent parameter determination. Parameters were estimated by minimizing an objective function, Φ [*Simunek et al.*, 1999], which represents deviations between measured and calculated space-time variables, and which was applied in a slightly simplified form as

$$\Phi(\boldsymbol{b}) = \sum_{j=1}^{m}\sum_{i=1}^{n} w_{i,j}\left[O_j(r, z, t_i) - E_j(r, z, t_i, \boldsymbol{b})\right]^2 \tag{3}$$

where m is the number of different sets of measurements, n represents the number of observations in a particular measurement set, $O_j(r, z, t_i)$ represents observations at time t_i for the j_{th} measurement set at location (r, z), $E_j(r, z, t_i, \boldsymbol{b})$ are the corresponding estimated space-time variables for the vector $\boldsymbol{b}$ of optimized *van Genuchten* [1980] parameters, and $w_{i,j}$ are weighting factors used here to account for differences in magnitude and number of data between different types of observations.

[16] To represent effects of the water flow direction, i.e., upward/downward infiltration and drainage, on the flow process (hysteresis), the model analysis required some of the hydraulic parameters to vary with the flow direction. On the other hand, for model simplicity it was desirable to constrain as many parameters as possible at constant values irrespective of the flow direction. In previous studies about soil hydraulic hysteresis, the residual and saturated water contents, θ_r and θ_s, and the parameter n in the *van Genuchten* [1980] model were sometimes fixed, resulting into a closed loop type hysteretic retention function [*Scott et al.*, 1983; *Simunek et al.*, 1998]. In other cases, θ_s was assumed to be smaller for infiltration than for drainage as a result of air entrapment below the infiltration front (open loop retention function) [e.g., *Aziz and Settari*, 1979; *Kool and Parker*, 1987]. Similarly, open or closed loop type hysteresis was also considered in the hydraulic conductivity function [*Vogel et al.*, 1996; *Simunek et al.*, 1998].

[17] Hysteresis in different pore domains during preferential flow has not yet been investigated in detail. In our parameter estimation procedure, we indirectly accounted for hysteretic hydraulic properties of matrix and macropore by allowing some of the ARE parameters to have different magnitudes for upward/downward infiltration and drainage, while other parameters were assumed as constant. The residual and saturated water contents, θ_r and θ_s, were fixed for matrix ($\theta_r = 0.2$, $\theta_s = 0.36$) and macropore ($\theta_r = 0.03$, $\theta_s = 0.35$). These values were obtained from standard multistep outflow measurements for separate homogeneous loam (matrix) and sand (macropore material) columns (J. M. Köhne et al., Inverse dual-permeability modeling of water flow in a soil column with a preferential flow path, submitted to *Vadose Zone Journal*, 2004) (hereinafter referred to as Köhne et al., submitted manuscript, 2004). Only the saturated matrix water content during downward infiltration was set to the corresponding value observed in the matrix of the column with macropore ($\theta_s = 0.33$). Additionally, the *van Genuchten* [1980] parameter n for the macropore domain was fixed at a value of 3.5 which on average gave the best results. Our empirical approach is equivalent to assuming an open loop hysteretic water retention function for the matrix and a closed loop water retention function for the macropore. A total number of 5 parameters had to be estimated to describe a particular

experiment; 3 for the matrix (α, n, K_s) and 2 for the macropore (α and K_s).

[18] The Levenberg-Marquardt algorithm was applied to minimize the weighted least squares of residuals between observations and model estimates (3) [*Simunek et al.*, 1999]. Using parameters derived from the inverse ARE simulation, forward simulations were performed with the three approaches DPM1, DPM2, and ECM (described below) as implemented into modified HYDRUS-1D [*Simunek et al.*, 1998, 2003]. For all models, initial and boundary conditions were chosen identical (Table 2). Furthermore, we minimized the effects of the numerical solution of the various models on the results by imposing identical vertical discretization, convergence criteria, and time step parameters. In this way the effect of the conceptual model-inherent differences on simulation results could be isolated and evaluated by direct comparison. In another study (Köhne et al., submitted manuscript, 2004), we compared dual-permeability water flow models, with parameters either inversely estimated or independently determined, with regard to their capability to simulate various flow experiments with macroporous soil column.

3.2. Dual-Permeability Models

[19] The DPM of *Gerke and van Genuchten* [1993a] with first-order water transfer term (DPM1) coupling the macropore and matrix flow domains as implemented into HYDRUS-1D [*Simunek et al.*, 1998, 2003] was alternatively provided with a second-order water transfer term (DPM2) [*Köhne et al.*, 2004]. DPM1 and DPM2 conceptually subdivide the bulk soil into two subdomains, the fracture continuum or macropore domain (subscript f) and the matrix domain (subscript m)

$$P = w_f P_f + (1 - w_f) P_m \tag{4}$$

where P may represent water content, water flux, or hydraulic conductivity (for equilibrium conditions), and w_f is the volumetric fraction of macropore domain ($0 < w_f < 1$). Two mixed-type Richards' equations describe transient water flow in macropore (5a) and matrix (5b)

$$\frac{\partial \theta_f}{\partial t} = \frac{\partial}{\partial z}\left(K_f \frac{\partial h_f}{\partial z} + K_f\right) - \frac{\Gamma_w}{w_f} \tag{5a}$$

$$\frac{\partial \theta_m}{\partial t} = \frac{\partial}{\partial z}\left(K_m \frac{\partial h_m}{\partial z} + K_m\right) + \frac{\Gamma_w}{1 - w_f} \tag{5b}$$

where Γ_w is the water transfer term (T^{-1}) (positive for macropore-to-matrix transfer direction). For DPM1 this is a first-order term defined as

$$\Gamma_w = \frac{\beta}{a^2} K_a \gamma_w (h_f - h_m) \tag{6}$$

where β is a dimensionless geometry coefficient, a is the half width of the matrix (L) or thickness of the matrix mantle in the case of hollow cylindrical geometry, K_a is the effective hydraulic conductivity at the macropore-matrix interface (LT^{-1}), and γ_w is a dimensionless scaling factor for which a value of 0.4 was recommended [*Gerke and van Genuchten*, 1993b], although γ_w to some degree depends on initial conditions and hydraulic properties of the matrix [*Gerke and van Genuchten*, 1993b] and macropore [*Castiglione et al.*, 2003]. Since for our carefully designed column (described earlier), wall coatings or dense/compact zones were absent at the macropore-matrix interface, we assumed that the function $K_a(h)$ was equal to $K_m(h)$. Therefore our calculation of K_a in the transfer term (6) differs slightly from that of *Gerke and van Genuchten* [1993b] as follows

$$K_a = 0.5\left(K_m(h_f) + K_m(h_m)\right) \tag{7}$$

For both DPM1 and DPM2, β was calculated assuming "hollow" cylindrical geometry for our sand-filled macropore according to *Gerke and van Genuchten* [1996] as

$$\beta = \frac{1}{[0.19 \ln(16\varsigma)]^2}; \qquad 1 < \varsigma < 100 \tag{8}$$

where the factor ζ was calculated as [*Gerke and van Genuchten*, 1996]

$$\varsigma = \frac{a + b}{b} \tag{9}$$

where b (L) is the radius of the cylindrical macropore. The volume fraction of the macropore domain, w_f, was calculated as

$$w_f = \frac{b^2}{(a + b)^2} = \frac{1}{\varsigma^2} \tag{10}$$

The DPM2 with second-order mass transfer term of *Zimmerman et al.* [1996] was given in a slightly modified form by *Köhne et al.* [2004]

$$\Gamma_w = \frac{\beta K_a}{2a^2} \frac{(h_f - h_m)\left[|h_m - h_i| + |h_f - h_i|\right]}{|h_m - h_i|} \tag{11}$$

where h_i is the initial pressure head assumed to be equal for matrix and macropore. The hydraulic conductivity K_a in (11) was evaluated according to *Köhne et al.* [2004] as

$$K_a = \frac{pK_m(h_m) + K_m(h_f)}{p + 1} \tag{12}$$

where p is a weighting factor, assumed to be equal to 17, since this value was found to be applicable for a range of hydraulic properties and initial conditions [*Köhne et al.*, 2004].

[20] The 1-D vertical numerical grid was discretized into 201 elements with a uniform node spacing of 0.4 cm. The system of two dual-permeability flow equations was solved sequentially for matrix and macropore domains using the Galerkin finite element method with program-controlled time steps to ensure convergence of the nonlinear equations both for matrix and macropore.

[21] Values for mass transfer related DPM parameters were derived from the experimental macropore-matrix geometry (a = 11 cm, b = 1.2 cm, ζ = 10.167, β = 1.0685, and

Table 3. van Genuchten Model Parameters for 3-D Axisymmetric Richards Equation (ARE) Approach Obtained by Inverse Estimation Using HYDRUS-2D[a]

Domain	θ_r,[b] cm^3 cm^{-3}	θ_s,[b] cm^3 cm^{-3}	α, cm^{-1}	n	K_s, cm d^{-1}
Infiltration Experiment					
Macropore	0.03	0.35	0.2151	3.5[b]	5275
Matrix	0.20	0.33	0.0057	1.69	1.36
Upward Infiltration Experiment					
Macropore	0.03	0.35	0.0631	3.5[b]	10907
Matrix	0.20	0.36	0.0065	1.40	2.47
Drainage Experiment					
Macropore[c]	0.03	0.35	0.3[d]	3.5[b]	14400[d]
Matrix[e]	0.20	0.36	0.0088	1.25	209.74

[a]See *Simunek et al.* [1999].
[b]Fixed (not fitted).
[c]At the bottom of the macropore, a hydraulic resistance layer (width d = 0.4 cm) was assumed with fitted K_s = 48.8 cm/d equivalent to a hydraulic resistance of $R = d/K_s$ = 0.0082 d.
[d]At upper constraint.
[e]At the bottom of the matrix, a 0.4 cm hydraulic resistance layer was assumed with fitted K_s = 0.24 cm/d (R = 1.66 d).

w_f = 0.009675). Furthermore, the water retention and hydraulic conductivity functions of matrix and macropore domains were calculated with *van Genuchten* [1980] equations using the parameters (Table 3) obtained with the ARE reference simulation. All model parameters were identically defined for DPM1 and DPM2 simulations.

3.3. Equivalent Continuum Model

[22] The equivalent continuum approach (ECM) was based on Richards' equation:

$$\frac{\partial \theta}{\partial t} = \frac{\partial}{\partial z}\left(K\frac{\partial h}{\partial z} + K\right) \tag{13}$$

In (13), superimposed *van Genuchten* [1980] functions representing a bimodal pore size distribution were assumed [*Durner*, 1994].

$$S_e(h) = \frac{\theta(h) - \theta_r}{\theta_s - \theta_r} = \sum_{i=1}^{k} w_i (1 + (\alpha_i |h|)^{n_i})^{-m_i} \tag{14}$$

$$K(\theta) = K_s \left(\sum_{i=1}^{k} w_i S_{e_i}\right)^{l} \frac{\left(\sum_{i=1}^{k} w_i \alpha_i \left[1 - \left(1 - S_{e_i}^{1/m_i}\right)^{m_i}\right]\right)^2}{\left(\sum_{i=1}^{k} w_i \alpha_i\right)^2} \tag{15}$$

Where S_e is the effective water content, the integer k denotes the number of subdomains, w_i are the weighting factors for the subcurves, and α_i, n_i, m_i and l are empirical parameters of the subcurves. Here the following assumptions are made to represent a porous medium with bimodal pore size distribution: k = 2, $w_1 = w_f$, $w_2 = 1 - w_f$, l = 0.5, $m_i = 1 - 1/n_i$, where parameters with subscript 1 and 2 represent macropore and matrix domains, respectively. As for the DPM1 and DPM2 approaches, van Genuchten parameters in individual domains were obtained from the inverse ARE reference solution (Table 3) and lumped as per (14) and (15).

[23] In the ARE approach, the flow divider at the lower end of the column was represented by a 5 cm high, 0.25 cm thick region with a zero hydraulic conductivity. In DPM1 and DPM2, K_a in the lowest 5 cm was set equal to zero. In the ECM approach, no flow divider could be considered.

4. Results and Discussion

4.1. Infiltration Experiment

[24] Figure 3 presents measurements of cumulative infiltration and outflow along with model results for ARE, DPM1, DPM2, and ECM for bulk soil column (Figure 3a) and measured versus simulated cumulative outflow out of macropore and matrix (Figure 3b). The initial outflow was exclusively from the macropore; matrix flow started an hour later (Figure 3b). Although the parallel increase of cumulative infiltration and outflow in Figure 3a suggests that steady state flow conditions were reached after 20 min, the later onset of matrix outflow reveals continuing transient flow conditions (Figure 3b). Agreement between simulations and observations was good for the ARE model (Figures 3a and 3b). Particularly DPM2, but also DPM1 (Figures 3a and 3b) and ECM (Figure 3a), approximated the ARE model results quite well. We note that individual fitting of the DPM and ECM parameters would have improved their agreement with data (not shown).

[25] Figure 4 shows observed and simulated pressure heads in the macropore, and in the matrix at 2 cm (transition region) and 6 cm (matrix domain) distance from the macropore wall at the depths of 5 cm (Figure 4a), 35 cm (Figure 4b), and 65 cm (Figure 4c). Within a particular region, pressure head reactions were observed sequentially at 5 cm, 35 cm, and 65 cm depths. Additionally, a lateral succession of pressure head reactions was observed in the order of macropore, transition region, and matrix (Figures 4a, 4b, and 4c). The ARE simulations showed the same spatial-temporal pattern as the observations in response to infiltration (Figure 4). As compared to the ARE approach, DPM1 predicted an early rise of macropore pressure heads and a late rise of matrix pressure heads (Figure 4), as DPM1 simulated an early start of macropore outflow and late start of matrix outflow (Figure 3b). The DPM2 approach more closely approximated the ARE-simulated matrix pressure head values, but predicted a late initial rise of macropore pressure heads. The ECM approach gave pressure heads for bulk porous medium that were between macropore and matrix pressure heads simulated with the ARE approach (Figures 4a, 4b, and 4c).

[26] The good description of the cumulative water flow data and relatively good approximation of domain-specific pressure heads suggested that the ARE approach was essentially suitable to describe the observed preferential infiltration process. The conceptual representation of the preferential flow process as assumed in the DPM approaches gave results that compared well for cumulative flow with some differences for domain-specific pressure heads. The simplified ECM approach approximated flow data reasonably well, but ECM can not distinguish between macropore and matrix flow which may lead to different solute transport prediction than using ARE or DPM approaches (not shown).

[27] The differences between the DPM1 and DPM2 approaches and ARE with respect to simulated flow

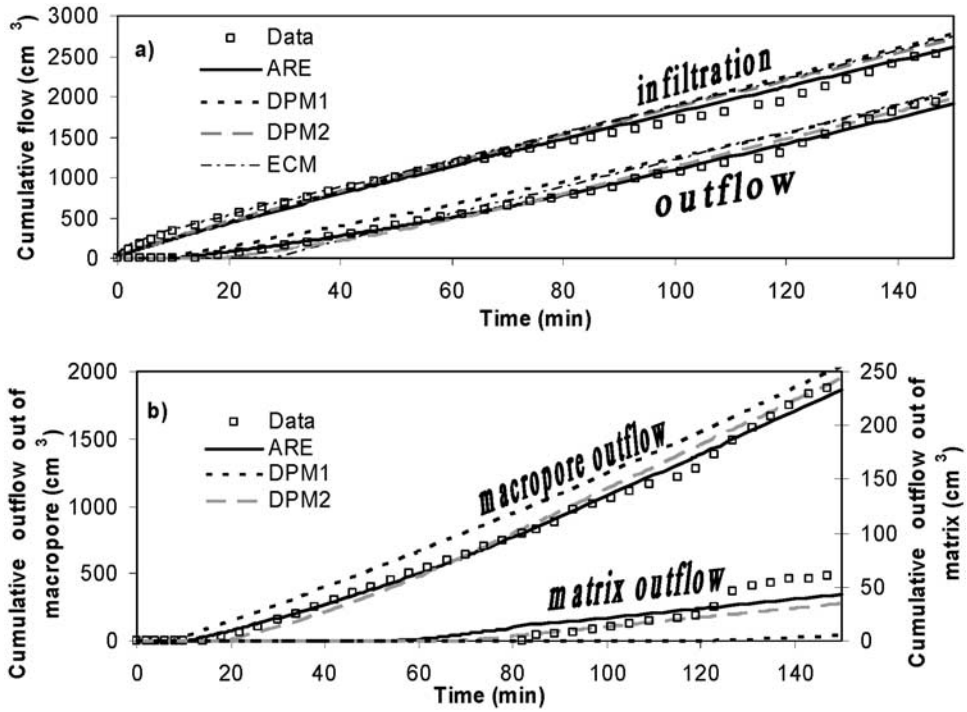

Figure 3. Data and simulations of the infiltration experiment: (a) cumulative infiltration and outflow (bulk soil) and (b) cumulative outflow out of macropore and matrix.

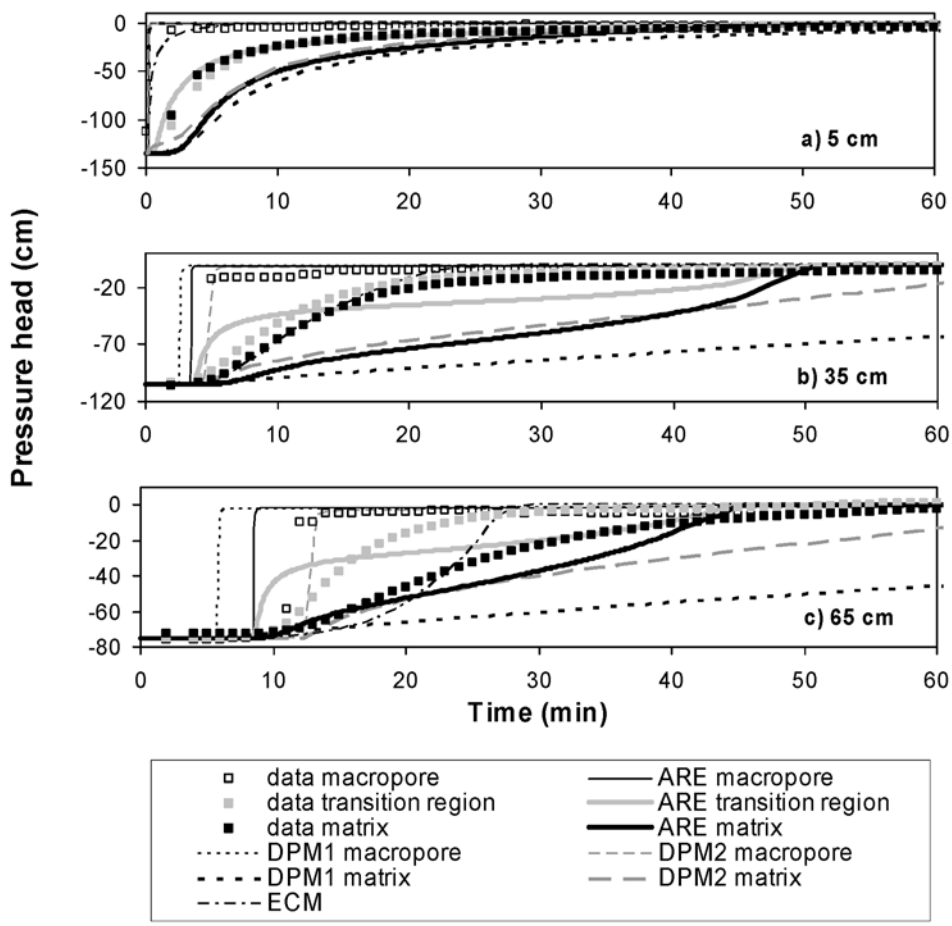

Figure 4. Data and simulations of the infiltration experiment: domain-specific pressure heads at depths of (a) 5 cm, (b) 35 cm, and (c) 65 cm.

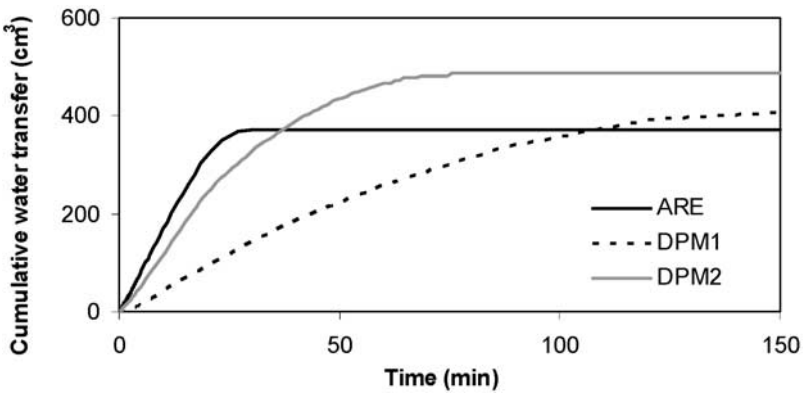

Figure 5. Simulations of the infiltration experiment: cumulative water transfer.

(Figure 3) and pressure heads (Figure 4) can for the most part be explained by differences in the calculated water transfer from macropore into matrix. For example, cumulative water transfer as simulated with ARE was initially underestimated by DPM1 (Figure 5). This between-domain water transfer underestimation led to the underestimation of matrix outflow and overestimation of macropore outflow (Figure 3b), and the corresponding early rise of DPM1 macropore pressure heads and late increase of matrix pressure heads (Figure 4).

4.2. Upward Infiltration Experiment

[28] Figure 6 compares the observed and simulated cumulative upward infiltration into the macropore. The infiltration was initially fast, but gradually reduced with time as the macropore and adjacent matrix approached saturation. The inverse ARE approach matched the measured upward infiltration well (Figure 6). The DPM2 approach gave a good approximation of the cumulative infiltration simulated with ARE. As compared to ARE, the DPM1 approach predicted a smaller early time infiltration, while the ECM overestimated early time infiltration and underestimated the final cumulative infiltration (Figure 6).

[29] Figure 7 presents measured and simulated water contents in the macropore at 20 cm depth (Figure 7a) and in the matrix at 50 cm depth (Figure 7b) and measured pressure heads at various depths in macropore, transition region, and matrix (Figure 7c). After only 5 min of infiltration, the TDR coil probe at the 20 cm depth recorded the maximum (saturated) macropore water content of 0.35 (Figure 7a). Water contents in the matrix at 50 cm depth reached their maximum values later (Figure 7b) in spite of being 30 cm closer to the upward infiltration boundary. The ARE approach could describe macropore water contents, but the total increase of matrix water contents (0.04) was somewhat underestimated using ARE (Figure 7b). Theoretically, however, an increase of matrix water contents by only 0.02 throughout the column would account for the total observed water infiltration (765 cm^3), which approximately corresponds to the simulated increase. The ECM approach simulated matrix soil water contents (Figure 7b) almost identical to ARE-simulated water contents in the transition region (not shown), which can be explained by the bimodal summation (14) of matrix and macropore retention functions. The DPM1 and DPM2 approaches gave matrix water contents close to those simulated with ARE for matrix (Figure 7b). Figure 7c reveals a fast succession of macropore pressure head increase between the 65 cm and 5 cm tensiometer positions, and a slower increase in matrix pressure head at the corresponding depths. The initial pressure heads reflected a static equilibrium profile. The final macropore pressure heads after 15 min represented dynamic equilibrium, where water was still transferred into the matrix as indicated by continued rise of matrix pressure heads after 15 min (Figure 7c).

[30] Figure 8 shows data and simulations of pressure heads in macropore and matrix at the depths of 20 cm (Figure 8a), 35 cm (Figure 8b), and 65 cm (Figure 8c). The general pattern of nonequilibrium between observed pressure heads could be reproduced by the ARE approach.

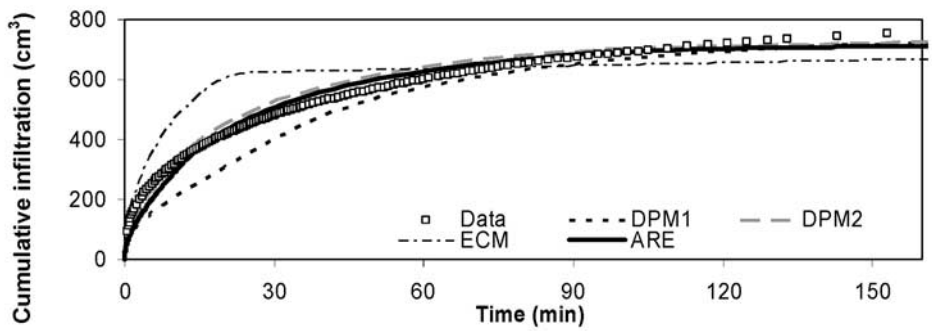

Figure 6. Data and simulations of the upward infiltration experiment: cumulative upward infiltration into the macropore.

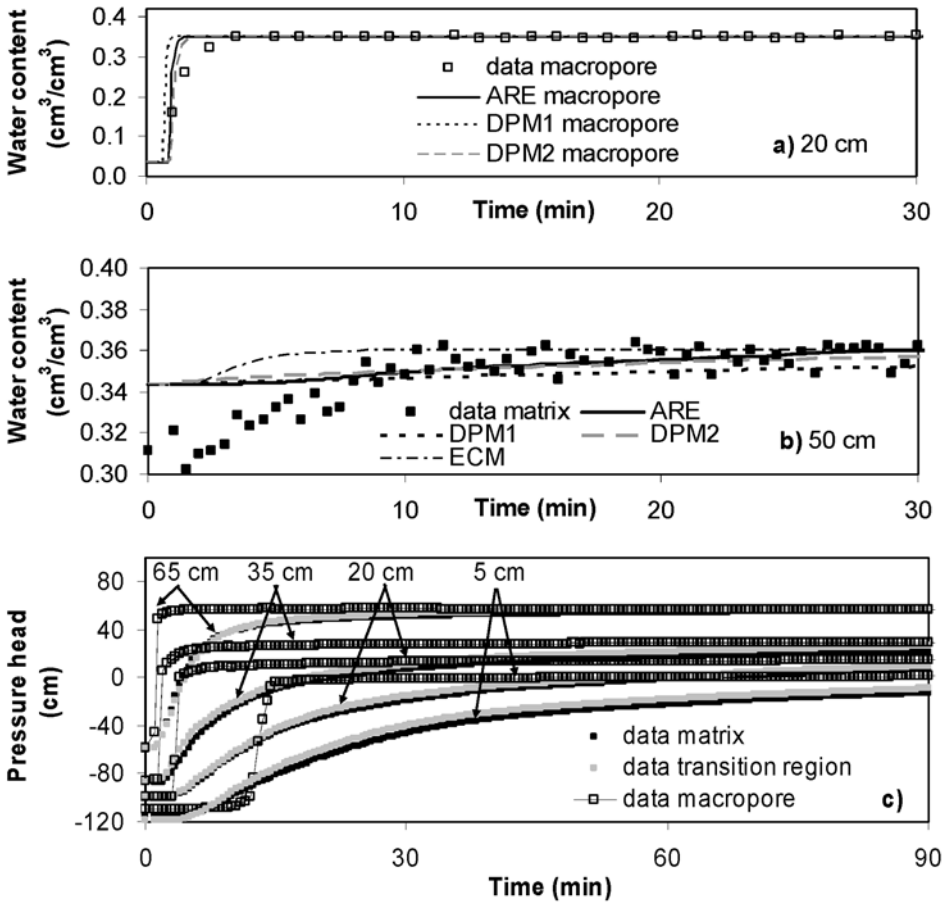

Figure 7. Data and simulations of the upward infiltration experiment: (a) macropore water contents at 20 cm depth, (b) matrix water contents at 50 cm depth, and (c) observed pressure heads at various positions.

However, ARE overestimated pressure head differences between the transition region and the matrix, and showed similar patterns of deviation from the observations as was found for downward infiltration (compare Figures 4 and 8). The DPM2 approach gave a closer representation than DPM1 of matrix pressure heads simulated using ARE. The ECM approach produced pressure heads between corresponding values in macropore and matrix simulated with the ARE approach. The ECM pressure heads reached steady state earlier than the DPM and ARE approaches (Figure 8) where macropore flow was delayed by between-domain water transfer.

[31] Figure 9 compares experimental and ARE simulated pressure heads in a vertical x-z plane at 1.5 min (Figure 9a), 6 min (Figure 9b), and 60 min (Figure 9c). The experimental pressure head profiles were calculated by linear interpolation between observations of 16 tensiometers and linear extrapolation for the area outside observation points. The simulated pressure head profile was obtained by linear interpolation between 4830 nodal values calculated with the ARE approach. Experimental and simulated pressure heads illustrate that the water front advanced much faster in the macropore than in the matrix (Figure 9). The effect of the flow divider near the lower boundary on pressure heads becomes apparent in the simulation results at early times (Figures 9a and 9b). On the contrary, due to limited observations near the lower boundary, this effect was not observed in the data. According to the ARE simulation, initially the matrix wetted only by lateral water transfer from the macropore as indicated by more vertical pressure head contour lines (Figures 9a and 9b). Later, since the matrix above the flow divider received transfer water from the macropore for a longer time at a higher rate (explained below), the matrix additionally got wetted by upward water movement in the matrix itself as indicated by horizontal contours (Figure 9c). The pronounced step in the ARE simulated matrix and transition zone pressure heads around 12 min at the 65 cm depth (Figure 8c) marks the shift at that depth from predominantly lateral wetting to additional upward wetting in the matrix.

[32] After 60 min, measured pressure heads in macropore and matrix were still slightly different in the upper part of the column indicating some remaining hydraulic nonequilibrium between the two domains (Figure 9c). In general, good agreement between the ARE results and observations is noted.

[33] In Figure 10, measured and simulated cumulative water transfer into the matrix (Figure 10a) and transfer rate profiles (Figure 10b) as simulated with ARE, DPM1, and DPM2 are shown. Water transfer was calculated from experimental data as the difference between measured infiltration into the macropore and the theoretical infiltration

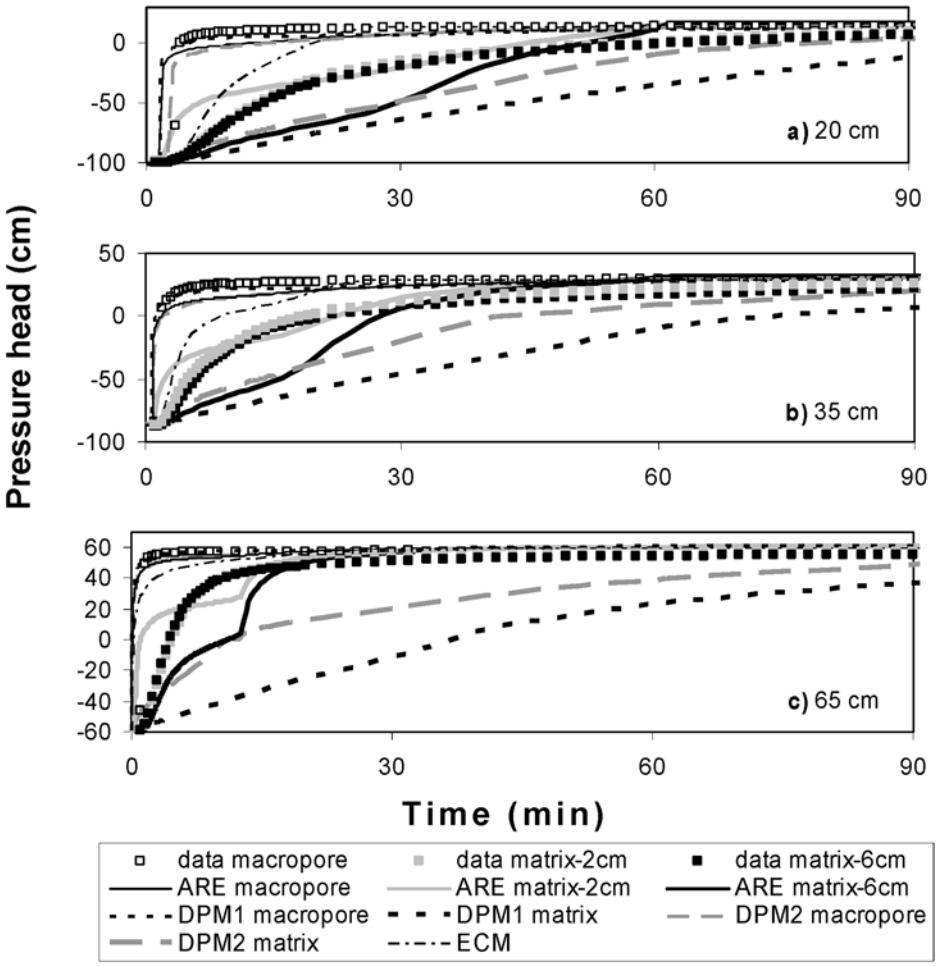

Figure 8. Data and simulations of the upward infiltration experiment: domain-specific pressure heads at (a) 20 cm depth, (b) 35 cm depth, and (c) 65 cm depth.

into the same macropore without transfer (Figure 10a). The theoretical infiltration into the macropore without transfer was estimated as the wetted macropore volume, $V_{macro} = \pi \times r^2 \times L \times (\theta_s - \theta_i)$, with the macropore radius r (1.2 cm), the wetted length L, the saturated (final) water content θ_s (0.35) (Figure 7) and the initial (residual) water content θ_i (0.03). The wetted length L was derived from tensiometer positions for the times when the tensiometers first showed positive pressure heads indicating full macropore saturation up to a particular tensiometer position. At the end of the experiment at 150 min, the macropore was wetted over its entire length with a V_{macro} of 115 cm^3. Water transfer into the matrix accounted for 650 cm^3 (765 cm^3 – 115 cm^3) or 85% of the total observed infiltration (765 cm^3) through the macropore inlet. Cumulative water transfer was accurately described by ARE (Figure 10a). The observed late time water transfer from macropore to matrix continuing past one hour (Figure 10a) was consistent with observed pressure head nonequilibrium after one hour (Figure 9c) and explains the observed late time infiltration (Figure 6). This late time water transfer behavior was reflected by the ARE, but less so by the DPM approaches. The DPM2 approach better than DPM1 approximated early time between-domain transfer calculated with ARE (Figure 10a). Figure 10b shows the transfer rate profiles obtained with the ARE, DPM2, and DPM1 approaches for different times (2, 20, and 60 min). For early times, ARE and DPM2 showed two peaks for water transfer; one at 75 cm depth above the flow divider, and the other at the upward infiltration front (Figure 10b). The water transfer peak at the 75 cm depth is caused by the large lateral hydraulic gradient between ponded macropore and adjacent unsaturated matrix pore space (Figure 9a). At 60 min, the DPM approaches failed to produce the transfer peak above the flow divider at 75 cm depth, since they can not simulate water transfer between two fully saturated regions. Attempts to allow for water transfer into a saturated region produced instability in the numerical solution and could not be employed in this study. However, part of our future work may concentrate on overcoming this shortcoming of water transfer calculations in DPM.

4.3. Drainage Experiment

[34] Observations and simulation results for the drainage experiment are shown in Figures 11 – 14. Figure 11 presents cumulative outflow of the macropore (Figure 11a), the matrix (Figure 11b), and the bulk soil (sum of matrix and macropore outflow, Figure 11c). Outflow from the macropore and the matrix started simultaneously, but at a higher rate for the

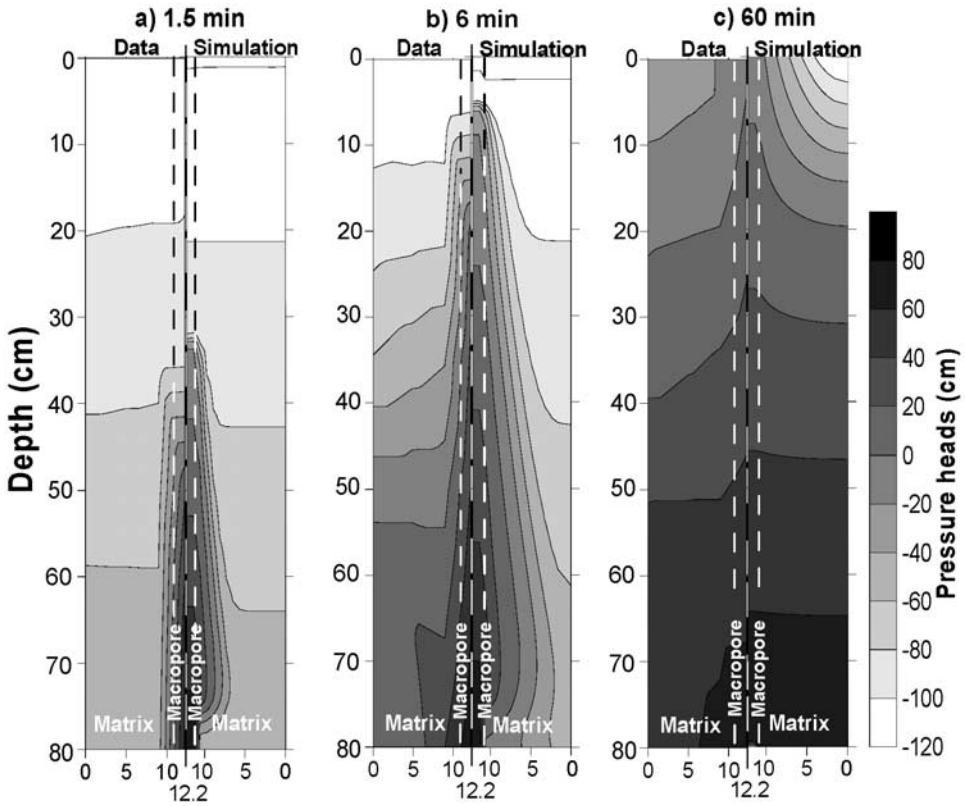

Figure 9. Data and simulations (ARE) of the upward infiltration experiment: pressure head profiles in half cross sections through the column at (a) 1.5 min, (b) 6 min, and (c) 60 min.

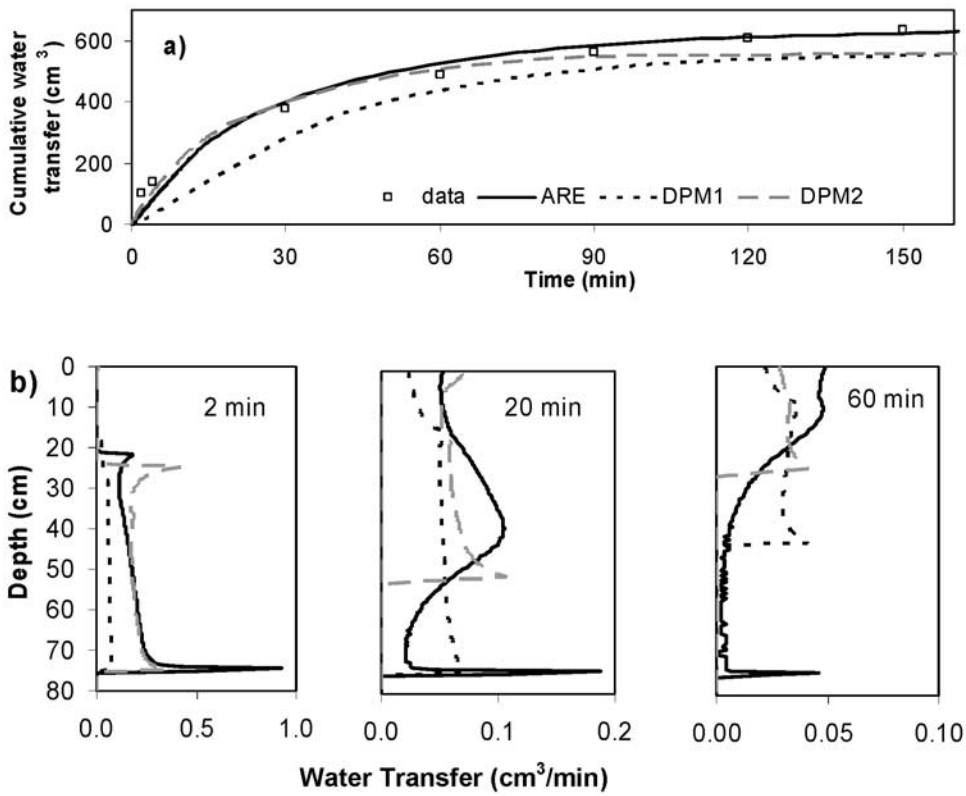

Figure 10. Data and simulations of the upward infiltration experiment: (a) cumulative water transfer and (b) water transfer rate profiles at 2, 20, and at 60 min.

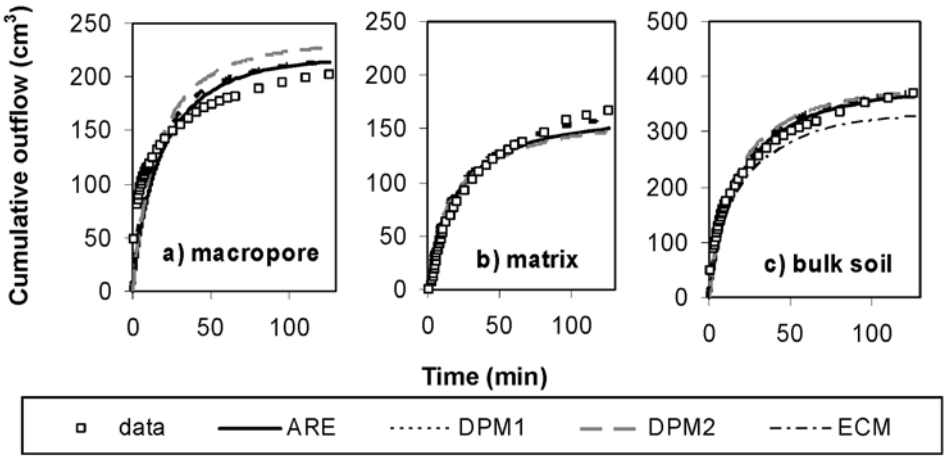

Figure 11. Data and simulations of the drainage experiment: (a) cumulative outflow from macropore, (b) cumulative outflow from matrix, and (c) cumulative outflow from bulk soil.

macropore (Figure 11a). Simulation results using the ARE approach were generally in good agreement with the observations (Figures 11a, 11b, and 11c). The DPM1 and DPM2 matched the ARE results for cumulative outflow out of bulk soil accurately (Figure 11c), however, DPM2 overestimated macropore outflow (Figure 11a) and DPM1 overestimated matrix outflow compared to ARE (Figure 11b). Among all approaches, only ECM did not match ARE results for bulk soil water outflow (Figure 11c).

[35] Figure 12 presents simulated and observed water contents at 35 cm depth in matrix and macropore. In the soil matrix water contents remained almost constant, whereas the TDR coil probe suggested that macropore water contents dropped from 0.34 to 0.1 within 10 min. However, from independent measurements of the coarse sand water retention function, the residual water content for coarse sand was known to be 0.03, which was assumed as the value for θ_r in the models. The TDR coil probe probably overestimated the water contents in the dry range. The initial drop of water content data was accurately simulated with all four modeling approaches.

[36] Data and model results of pressure heads in three different flow domains at 35 cm and 65 cm depths are illustrated in Figures 13a and 13b. The observed pressure heads started with positive values. The only way to reproduce initial positive pressures with the Richards' equation based models was to assume an outflow resistance across the lower boundary. In the drainage experiment, the lower boundary with a nylon membrane (30 μm mesh size) between two hole plates may indeed have caused some hydraulic resistance. For the upward/downward infiltration experiments, one of the hole plates was removed and the nylon membrane was replaced with cheesecloth, such that hydraulic resistance was assumed to be negligible. We note, however, that early time positive pressure heads were even encountered in replicate drainage experiments without nylon membrane at the bottom (not shown). Hence other phenomena may have additionally contributed to the gradual decrease of positive pressures during drainage, which should be investigated more closely in future. In this study, lacking additional information, positive pressures were assumed to be entirely caused by outflow resistance across the bottom boundary. Matrix pressure heads in the upper half of the column (at 35 cm depth) dropped below macropore pressure heads (Figure 13a), whereas matrix pressure heads in the lower half of the column (at 65 cm depth) were converging to similar values (Figure 13b). The ARE approach reproduced pressure heads in matrix, transition, and macropore domains at both 35 cm (Figure 13a) and at 65 cm (Figure 13b) depth,

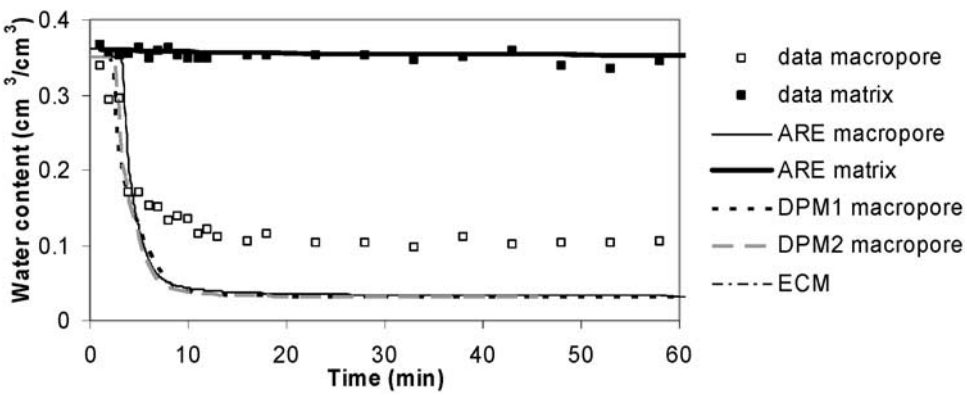

Figure 12. Data and simulations of the drainage experiment: water contents at 35 cm depth in matrix and macropore.

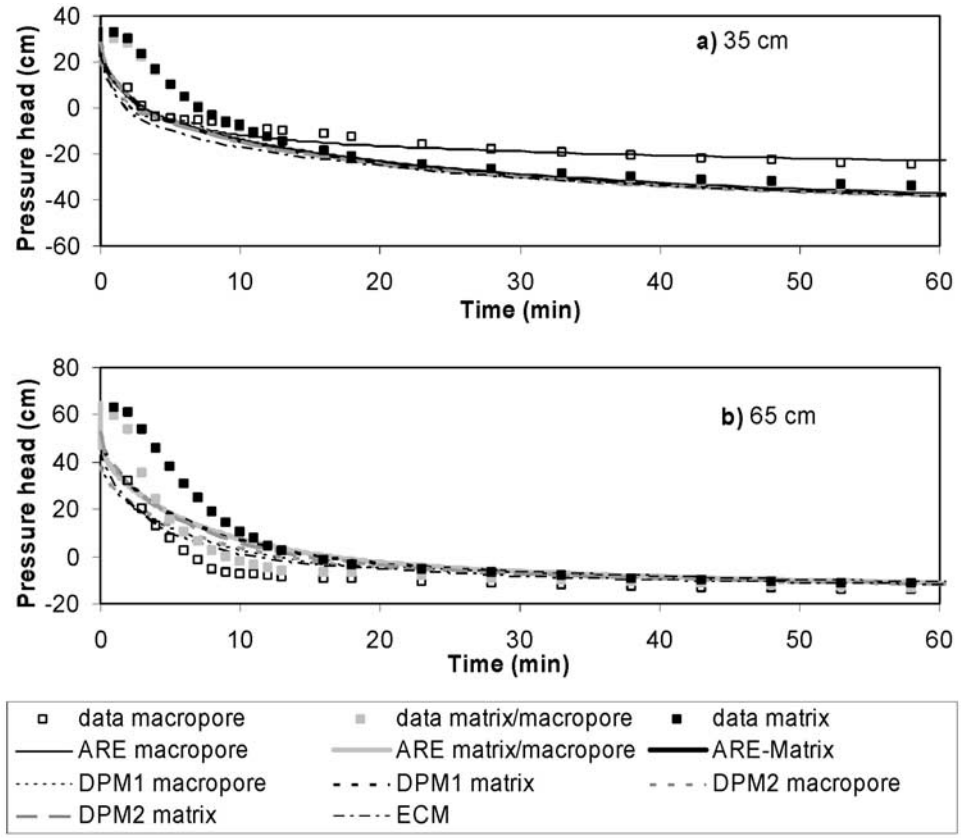

Figure 13. Data and simulations of the drainage experiment: domain-specific pressure heads at depths of (a) 35 cm and (b) 65 cm.

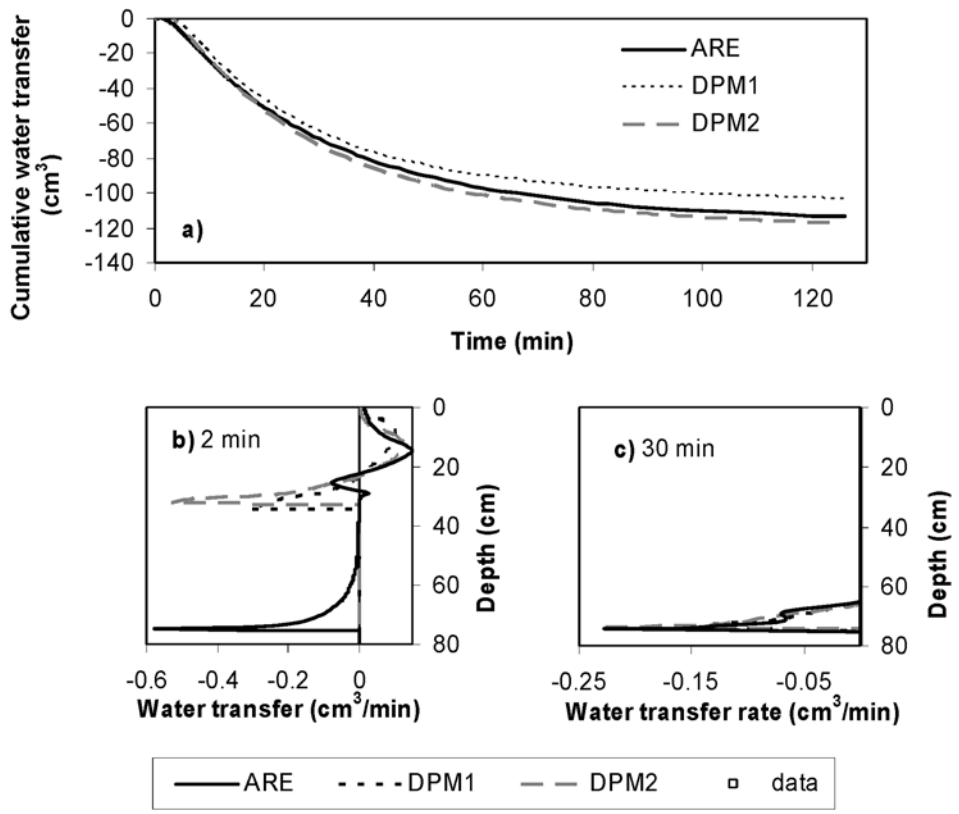

Figure 14. Data and simulations of the drainage experiment: (a) cumulative water transfer from matrix into macropore and profiles of water transfer rate at (b) 2 min and (c) 30 min.

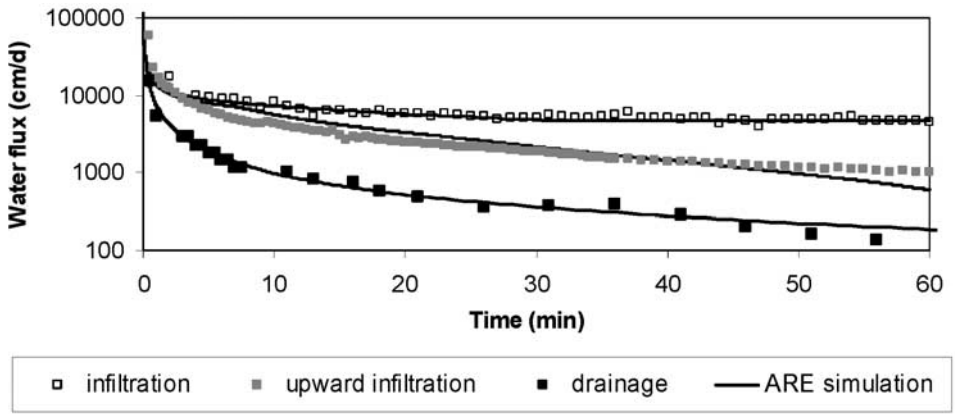

Figure 15. Measured macropore water fluxes during drainage, infiltration, and upward infiltration and corresponding simulated water fluxes using the ARE approach.

except that it could not describe interregion differences in pressure heads (Figures 13a and 13b). The pressure heads simulated using the DPM (ECM) approaches closely approximated region-specific (matrix) pressure heads obtained with the ARE approach (Figure 13).

[37] Figure 14 shows cumulative water transfer estimated from experimental data and simulation results for the ARE, DPM1 and DPM2 approaches (Figure 14a), and simulated depth profiles of water transfer at 2 min (Figure 14b) and 30 min (Figure 14c). The initially completely saturated macropore was estimated to drain 115 cm^3 of water (i.e., 4.52 $cm^2 \times 80$ cm $\times$ (0.35−0.03)) without water transfer. Since the cumulative outflow out of the macropore totaled 201 cm^3 after 125 min (Figure 11a), water transfer from the matrix must have contributed 86 cm^3, corresponding to 43% of macropore outflow. Cumulative water transfer after 125 min as simulated with ARE (114 cm^3) overestimated cumulative transfer, while DPM approaches were in good agreement with the ARE approach (Figure 14a). Simulated depth profiles of the water transfer rate at 2 min (Figure 14b) illustrate the complex early time pattern of water transmitted back and forth between matrix and macropore throughout the profile at relatively high rates. The complex water transfer pattern resulted from the pressure head depth distribution in macropore and matrix as modified by hydraulic resistances at the lower boundary. The models predicted that although the macropore drained faster than the matrix (and water contents decreased faster), pressure heads decreased more slowly for a certain pressure range depending on the water retention function (not shown). Hence, in part of the profile the horizontal hydraulic gradient was directed from macropore into matrix. At 30 min, there was only matrix-to-macropore water transfer confined to the lower half of the profile at lower rates (Figure 14b). As was found for the upward infiltration case (Figure 10b), the DPM approaches at 2 min (following initiation of drainage of the saturated column) could not reproduce the sharp water transfer peak obtained with ARE between saturated regions above the flow divider (Figure 14b). The DPM models simulated water transfer in the unsaturated zone above the 35 cm depth (i.e., drainage front) (Figure 14b).

[38] Because of the underestimation of lateral water transfer into the macropore (Figures 14a and 14b), simulated matrix flow using DPM1 slightly exceeded ARE-simulated matrix flow at 125 min (Figure 11b). Overall, as for the other examples, DPM2 gave simulation results slightly closer to ARE than DPM1.

4.4. Was the Assumption of Darcy's Law Valid?

[39] For testing the validity of the viscous flow assumption as required by the models in this study based on Darcy's law, experimental water fluxes in the macropore were analyzed. Measured and simulated (ARE) macropore water fluxes for drainage and downward and upward infiltration are shown in Figure 15. The highest initial flux of 60,000 cm d^{-1} was found for upward infiltration due to the high initial pressure head gradient (Figure 15). The ARE approach matched well both with high initial macropore water fluxes and later steady state (infiltration) or decreasing (upward infiltration, drainage) macropore water fluxes (Figure 15). To assess if water flow may have been affected by inertial forces, Reynolds' number, R_e (dimensionless), was estimated for the highest macropore flux encountered during each experiment using (16) [*Hillel*, 1998]

$$R_e = \frac{v_f\, d}{\eta} \tag{16}$$

where v_f [LT^{-1}] is the pore water velocity, $v_f = q_f/(\theta_{f,s} - \theta_{f,r})$ with q_f [LT^{-1}] as the macropore water flux, d [L] is the effective particle diameter of the coarse sand in the macropore, and η is the viscosity [$MT^{-1}L^{-1}$]. Assuming that $d = 0.001$ m, $\eta = 0.001$ kg $s^{-1}m^{-1}$, $(\theta_{f,s} - \theta_{f,r}) = 0.3$ and q_f as measured in a particular experiment, maximum calculated values for R_e ranged between 6 (drainage, infiltration) and 18 (upward infiltration). For a Reynolds number less than unity, the flow is viscous and no significant inertial forces are present. For all experiments, Reynolds' numbers dropped to values below one within few minutes (after initiation of a particular experiment), such that except during very early times, there was entirely viscous flow as assumed in Darcy's law.

4.5. Domain-Specific and Composite Hydraulic Functions

[40] The hydraulic functions for matrix and macropore domains as obtained by fitting the ARE approach to the data of infiltration, drainage, and upward infiltration, are shown in Figure 16. The domain-specific *van Genuchten* [1980] model parameters are listed in Table 3. Figure 16 illustrates

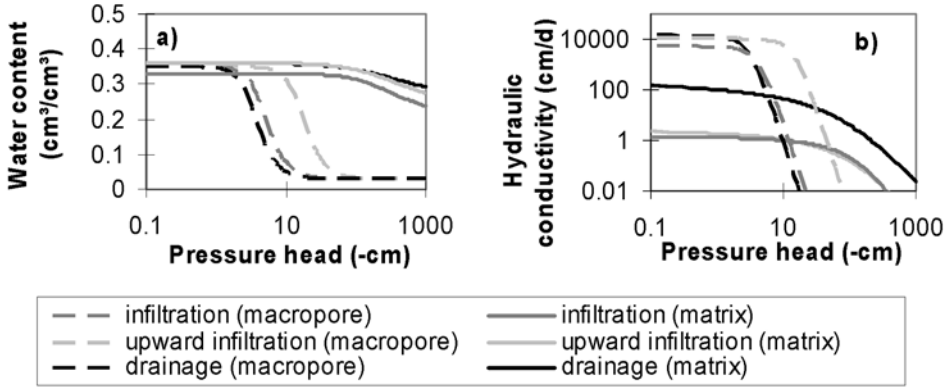

Figure 16. Hydraulic van Genuchten functions for matrix and macropore obtained by inverse parameter estimation of approach ARE for drainage, infiltration, and upward infiltration experiments: (a) water retention and (b) hydraulic conductivity.

the distinct differences between hydraulic properties of matrix and macropore. These differences were reflected by parameter values of α, n, and K_s being consistently higher (by three orders of magnitude for K_s) for the macropore than for the matrix (Table 3). For upward and downward infiltration, the matrix hydraulic functions were quite similar (Figures 16a and 16b). By contrast, macropore hydraulic conductivities showed higher values for upward than for downward infiltration, and the same trend was found for macropore water contents except at saturation (Figures 16a and 16b). A possible explanation for the somewhat lower macropore hydraulic conductivities and water contents during downward infiltration would be air entrapment. For downward infiltration and drainage, the two pore region retention functions (Figure 16a) and the macropore hydraulic conductivity (Figure 16b) showed only small differences. However, the matrix hydraulic conductivity was much higher for drainage than for (downward) infiltration (Figure 16b) and was probably overestimated, in part compensating for the flow resistance at the lower boundary.

[41] Figure 17 shows the composite water retention functions (Figure 17a) and hydraulic conductivity functions (Figure 17b) calculated as weighted sums of the estimated individual matrix and macropore functions using equation (4). Figure 17 illustrates that composite water retention functions (Figure 17a) differed much less for different flow experiments than did composite hydraulic conductivity functions (Figure 17b). For upward/downward infiltration, this difference of composite hydraulic conductivity arose from differences in the macropore hydraulic functions only (Figure 16b).

[42] Figure 17 further illustrates that even for a distinct dual-permeability medium, double-hump shape with two inflection points may not become obvious from bulk soil retention functions, $\theta(\log h)$ (Figure 17a). By contrast, if there was a cross-over point where the macropore conductivity fell below matrix conductivity as was the case for all examples (Figure 16b), $\log K(\log h)$ clearly showed two inflection points (Figure 17b). These findings corroborate similar results found by *Köhne et al.* [2002] for undisturbed, structured loamy soil columns as well as the findings of *Mohanty et al.* [1997] in a field soil in New Mexico.

5. Conclusions

[43] A novel soil column setup allowed us to monitor preferential water flow processes locally in the cylindrical sand-filled preferential flow path (macropore) and the surrounding repacked loamy matrix mantle. The experiments demonstrated that local hydraulic nonequilibrium of pressure heads, water contents and flow velocities in matrix and macropore domains are characteristics of preferential flow. Cumulative, depth-integrated interdomain transfer could be estimated using simple mass balance calculations. Four numerical flow models of different complexity based on Richards' equation were evaluated using the domain-specific preferential water flow data. The most accurate

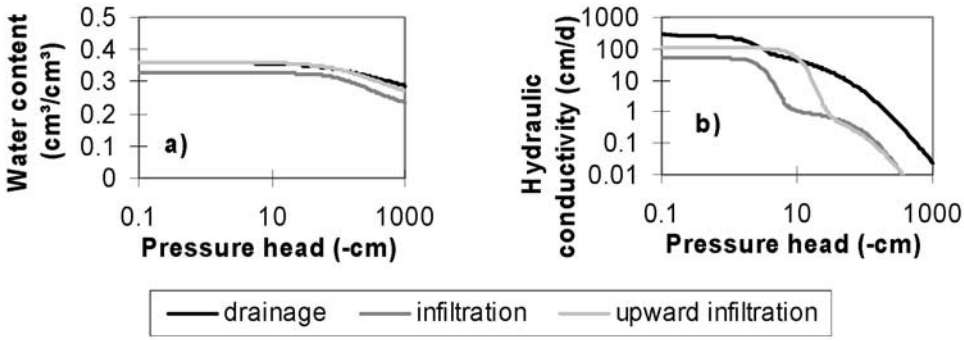

Figure 17. Hydraulic van Genuchten functions for bulk soil obtained by summing up macropore and matrix functions of Figure 13: (a) water retention and (b) hydraulic conductivity.

modeling approach was three-dimensional axisymmetric Richards' equation with inverse parameter identification. The analysis of experimental data using this benchmark model produced hydraulic functions that were distinctly different for the macropore and the matrix domains. The results further suggest that preferential flow processes may be affected by the flow direction, and that accurate simulation of preferential flow may require consideration of hysteresis in flow regions. Furthermore, the results demonstrate that the composite or bulk soil hydraulic conductivity functions display double-hump shape if there is a crossover point between the domain-specific hydraulic functions, whereas double-hump shape is less obvious in water retention functions.

[44] The equivalent continuum model based on Richards' equation with bimodal hydraulic functions gave results that were deemed to be acceptable. However, ECM's accuracy is somewhat lower than the other modeling approaches. The results of this study suggest that dual-permeability models based on Richards' equation are capable of simulating low Reynolds' number type preferential water flow. The second-order transfer term in the dual-permeability model may lead to somewhat more accurate simulation of preferential flow than the first-order term. The effect of using a second-order term for water transfer calculation may be more pronounced for other geometries than the cylindrical macropore geometry used in this study and needs further evaluation.

[45] **Acknowledgments.** This project has been supported by the National Science Foundation (grant EAR 0296158). We thank Jirka Simunek for assisting us with various modifications of the HYDRUS-1D and HYDRUS-2D codes used in this study.

References

Ahuja, L. R., K. E. Johnson, and G. C. Heathman (1995), Macropore transport of a surface-applied bromide tracer: Model evaluation and refinement, *Soil Sci. Soc. Am. J.*, *59*, 1234–1241.

Allaire, S. E., S. C. Gupta, J. Nieber, and J. F. Moncrief (2002a), Role of macropore continuity and tortuosity on solute transport in soils: 1. Effects of initial and boundary conditions, *J. Contam. Hydrol.*, *58*, 299–321.

Allaire, S. E., S. C. Gupta, J. Nieber, and J. F. Moncrief (2002b), Role of macropore continuity and tortuosity on solute transport in soils: 2. Interactions with model assumptions for macropore description, *J. Contam. Hydrol.*, *58*, 283–298.

Allaire-Leung, S. E., S. C. Gupta, and J. F. Moncrief (2000a), Water and solute movement in soil as influenced by macropore characteristics: 1. Macropore continuity, *J. Contam. Hydrol.*, *41*, 283–301.

Allaire-Leung, S. E., S. C. Gupta, and J. F. Moncrief (2000b), Water and solute movement in soil as influenced by macropore characteristics: 1. Macropore tortuosity, *J. Contam. Hydrol.*, *41*, 303–315.

Aziz, K., and A. Settari (1979), *Petroleum Reservoir Simulation*, Appl. Sci., London.

Bouma, J., and J. L. Anderson (1977), Water and chloride movement through soil columns simulating pedal soils, *Soil Sci. Soc. Am. J.*, *41*, 766–770.

Castiglione, P., B. P. Mohanty, P. J. Shouse, J. Simunek, M. T. Van Genuchten, and A. Santini (2003), Lateral water diffusion in an artificial macroporous system: Modeling and experimental evidence, *Vadose Zone J.*, *2*, 212–221.

Durner, W. (1994), Hydraulic conductivity estimation for soils with heterogeneous pore structure, *Water Resour. Res.*, *30*(2), 211–223.

Ela, S. D., S. C. Gupta, and W. J. Rawls (1992), Macropore and surface seal interactions affecting water infiltration into soil, *Soil Sci. Soc. Am. J.*, *56*, 714–721.

Gerke, H. H., and M. T. van Genuchten (1993a), A dual-porosity model for simulating the preferential movement of water and solutes in structured porous media, *Water Resour. Res.*, *29*, 305–319.

Gerke, H. H., and M. T. van Genuchten (1993b), Evaluation of a first-order water transfer term for variably saturated dual-porosity flow models, *Water Resour. Res.*, *29*, 1225–1238.

Gerke, H. H., and M. T. van Genuchten (1996), Macroscopic representation of structural geometry for simulating water and solute mass transfer in dual-porosity media, *Adv. Water Resour.*, *19*, 343–357.

Ghodrati, M., M. Chendorain, and Y. J. Chang (1999), Characterization of macropore flow mechanism in soil by means of a split macropore column, *Soil Sci. Soc. Am. J.*, *63*, 1093–1101.

Hillel, D. (1998), *Environmental Soil Physics*, 771 pp., Elsevier, New York.

Köhne, J. M., S. Köhne, and H. H. Gerke (2002), Estimating the hydraulic functions of dual-permeability models from bulk soil data, *Water Resour. Res.*, *38*(7), 1121, doi:10.1029/2001WR000492.

Köhne, J. M., B. P. Mohanty, J. Simunek, and H. H. Gerke (2004), Numerical evaluation of a second-order water transfer term for variably saturated dual-permeability models, *Water Resour. Res.*, *40*, W07409, doi:10.1029/2004WR003285.

Kool, J. B., and J. C. Parker (1987), Development and evaluation of closed-form expressions for hysteretic soil properties, *Water Resour. Res.*, *23*(1), 105–114.

Li, Y., and M. Ghodrati (1997), Preferential transport of solute through soil columns containing constructed macropores, *Soil Sci. Soc. Am. J.*, *61*, 1308–1317.

Logsdon, S. D. (1995), Flow mechanisms through continuous and buried macropores, *Soil Sci.*, *160*(4), 237–242.

Mohanty, B. P., R. S. Bowman, J. M. H. Hendrickx, and M. T. van Genuchten (1997), New piecewise-continuous hydraulic functions for modeling preferential flow in an intermittent-flood-irrigated field, *Water Resour. Res.*, *33*(9), 2049–2063.

Nissen, H. H., P. Moldrup, and K. Henriksen (1998), High-resolution time-domain reflectometry coil probe for measuring soil water content, *Soil Sci. Soc. Am. J.*, *62*, 1203–1211.

Nissen, H. H., P. Moldrup, L. W. de Jonge, and O. H. Jacobsen (1999), Time-domain reflectometry coil probe measurements of water content during finger flow, *Soil Sci. Soc. Am. J.*, *63*, 493–500.

Ray, C., T. R. Ellsworth, A. J. Valocchi, and C. W. Boast (1997), An improved dual porosity model for chemical transport in macroporous soils, *J. Hydrol.*, *193*, 270–292.

Scott, P. S., G. J. Farquhar, and N. Kouwen (1983), Hysteresis effects on net infiltration: Advances, *Publ.11-83*, pp. 163–170, Am. Soc. Agric. Eng., St. Joseph, Mich.

Simunek, J., M. Sejna, and M. T. van Genuchten (1998), The HYDRUS-1D software package for simulating the one-dimensional movement of water, heat, and multiple solutes in variably-saturated media, version 2.0, *IGWMC-TPS-70*, 202 pp., Int. Ground Water Model. Cent., Colo. Sch. of Mines, Golden.

Simunek, J., M. Sejna, and M. T. van Genuchten (1999), The HYDRUS-2D software package for simulating two-dimensional movement of water, heat, and multiple solutes in variably-saturated media, version 2.0, *IGWMC-TPS-53*, 251 pp., Int. Ground Water Model. Cent., Colo. Sch. of Mines, Golden.

Simunek, J., N. J. Jarvis, M. T. van Genuchten, and A. Gärdenäs (2003), Review and comparison of models for describing nonequilibrium and preferential flow and transport in the vadose zone, *J. Hydrol.*, *272*, 14–35.

van Genuchten, M. T. (1980), A closed-form equation for predicting the hydraulic conductivity of unsaturated soils, *Soil Sci. Soc. Am. J.*, *44*, 892–898.

Vogel, T., K. Huang, R. Zhang, and M. T. van Genuchten (1996), The HYDRUS code for simulating one-dimensional water flow, solute transport, and heat movement in variably-saturated media, version 5.0, *Res. Rep. 140*, U.S. Salinity Lab., Agric. Res. Serv., Riverside, Calif.

Wang, Z., A. Tuli, and W. A. Jury (2003), Unstable flow during redistribution in homogeneous soil, *Vadose Zone J.*, *2*, 52–60.

Zimmerman, R. W., T. Hadgu, and G. S. Bodvarsson (1996), A new lumped-parameter model for flow in unsaturated dual-porosity media, *Adv. Water Resour.*, *19*(5), 317–327.

J. M. Köhne and B. P. Mohanty, Department of Biological and Agricultural Engineering, Texas A&M University, Scoates Hall, College Station, TX 77843-2117, USA. (mkoehne@cora.tamu.edu; bmohanty@tamu.edu)